Available online at www.sciencedirect.com
ScienceDirect
Journal of Power Sources 171 (2007) 282–293
JOURNAL OF POWER SOURCES
www.elsevier.com/locate/jpowsour

Experimental and modelling studies of CO poisoning in PEM fuel cells

C.G. Farrell [a], C.L. Gardner [a,*], M. Ternan [b]

[a] *Department of Chemical Engineering and Centre for Catalysis Research and Innovation, University of Ottawa, Ottawa, Ontario K1N 6N5, Canada*
[b] *EnPross Inc., 147 Banning Road, Ottawa, Ontario K2L 1C5, Canada*

Received 17 May 2007; received in revised form 4 July 2007; accepted 5 July 2007
Available online 10 July 2007

Abstract

This article is an examination of the CO poisoning and cleaning (stripping) phenomenon that occur in a PEM fuel cell operating on an impure hydrogen stream such as reformed hydrocarbons or alcohols. A range of experimental results including cell polarization curves, measurements of spontaneous and transient oscillations of the anode potential and current pulsing behaviour are presented. Detailed examination of the pulsing process has shown that optimization of both the pulse width and pulse initiation potential will have an important impact on the overall fuel cell efficiency. To optimize these processes, the development of a mathematical model to understand and control the poisoning and cleaning processes is going to be important. In this paper, we have extended the model of Zhang et al. [J. Zhang, Investigation of CO tolerance in proton exchange membrane fuel cells, PhD thesis, Worcester Polytechnic Institute, June, 2004; J. Zhang, R. Datta, J. Electrochem. Soc. 149 (2002) A1423; J. Zhang, J.D. Fehribach, R. Datta, J. Electrochem. Soc. 151 (2004) A689] to include mass transfer effects. It is shown that this new model gives results that are in reasonable agreement with our experimental data.

Keywords: CO poisoning; PEM fuel cell; Oscillations; Periodic pulsing

1. Introduction

In recent years, there has been considerable interest in the development of proton exchange membrane (PEM) fuel cells for transportation and stationary applications. In the short to medium time frame, the major source of hydrogen for such applications is expected to come from hydrocarbon reformation principally because of its low cost and, for transportation applications, the ease of storage of a liquid fuel such as methanol. These hydrocarbon derived fuel streams inevitably contain significant levels of carbon monoxide that poisons the anode catalyst and degrades fuel cell performance [1,2]. The effect of CO on the steady state polarization curves of PEM fuel cells has been the studied [3]. It has been shown that even relatively low levels of CO contamination (5–10 ppm) can cause significant performance degradation. In addition to the steady state degradation of the performance of a PEM fuel cell, CO poisoning can also result in a variety of transient effects including, under certain conditions, spontaneous oscillations in cell potential [4–6].

The general mechanism of CO poisoning of a platinum or platinum alloy catalyst is well understood [7–9]. As shown below (Eqs. (1)–(3)), CO competes with hydrogen for the reaction sites on the platinum at normal anode operating potentials:

$$H_2 + 2S \leftrightarrow 2H\text{–}S \quad (1)$$

$$2H\text{–}S \leftrightarrow 2S + 2H^+ + 2e^- \quad (2)$$

$$CO + S \leftrightarrow CO - S \quad (3)$$

where S represents a catalytic site on the electrode. With even relatively low levels of CO, the catalyst surface is largely blocked by CO due to a higher affinity. This leaves a relatively small portion of the surface available for hydrogen adsorption. This raises the effective current density which polarizes the cell and results in low cell potential and poor overall fuel cell efficiency. As an example, the work of Papageorgopoulos and de Bruijn [10] shows that, for a 1% CO/hydrogen mixture, CO blocks 98% of the reaction sites at 25 °C.With a pure platinum catalyst, the adsorbed CO on a catalytic site can be removed by raising the anode potential to about 700 mV versus RHE. At this potential, as shown in Eqs. (4) and (5), the adsorbed CO reacts with hydroxyl species that are formed on the platinum surface to form

* Corresponding author. Tel.: +1 613 832 3689.
E-mail address: cgardner88@sympatico.ca (C.L. Gardner).

0378-7753/$ – see front matter © 2007 Elsevier B.V. All rights reserved.
doi:10.1016/j.jpowsour.2007.07.006

CO_2:

$$H_2O + S \leftrightarrow OH\text{–}S + H^+ + e^- \quad (4)$$

$$CO\text{–}S + OH\text{–}S \rightarrow 2S + CO_2 + H^+ + e^- \quad (5)$$

Operation of the fuel cell at the high anode potential required for the formation of OH on the platinum surface is impractical because the efficiency is very low under these conditions. To overcome this problem, various methods have been proposed to alleviate CO poisoning in PEM fuel cells including:

(a) Air bleeding

To prevent poisoning, CO levels need to be kept at a very low (~5 ppm) level. This requires the use of both shift and preferential oxidation (PrOx) reactors following the steam reforming stage of hydrogen generation, which add complexity and cost to the fuel cell system. Even when these additional stages are used, it is difficult to maintain low CO levels during start-up and transient operation without using an additional air bleed [11,12] into the fuel stream. Although air bleeding can remove CO, it has some disadvantages. Air bleeding into a fuel cell stack can cause overheating at the anode if the air is not controlled and mixed properly and can result in the formation of hydrogen peroxide which can lead to membrane degradation.

(b) Use of CO tolerant catalysts

To try to overcome the CO poisoning problem, bifunctional platinum-alloy catalysts such as Pt/Ru have been developed [7,8]. With these catalysts, the formation of adsorbed OH occurs on the alloy component more easily and the CO oxidation reactions, as per Eqs. (4) and (5), occur at substantially lower anode potential. In spite of a substantial improvement, the use of CO tolerant catalysts such as Pt/Ru still results in a significant loss of cell potential because of CO fouling. The results of Iorio et al. [13] show that, while the use of Pt/Ru results in a significant reduction of anode potential when compared to pure platinum (a decrease of about 250 mV), there is still a loss of about 200 mV (or a loss of 30% in potential efficiency) when compared with the use of pure hydrogen as a fuel.

(c) Periodic pulsing of the anode potential

Periodic pulsing of the anode is also a method for improving the performance [14] of a fuel cell that uses reformate as a fuel. The review by Wasmus and Kuver [15] identified a patent by Stimming, Friedrich, and Unkauf that described the application of short current pulses to remove residues, restore initial catalytic activity, and thereby circumvent CO poisoning. In this method, the applied pulse briefly raises the anode potential to a sufficiently high level so that CO can be oxidized to CO_2. This frees the surface from the CO poison and allows the anode potential to fall. This pulse technique can significantly increase the operating efficiency of the fuel cell. Most commonly, the pulse is provided electrically [14] by momentarily increasing the cell current. The careful control of each cell's potential that this approach requires has limited its use in large fuel cell stacks. When uniform pulsing is done on a stack of fuel cells in series, the variations in voltage across the cells can result in the weak cells being forced into reversal. A method that allows each cell in a stack to be separately pulsed under controlled conditions has been developed [16] to overcome this problem. Wilkinson et al. [17] have also proposed the use of periodic fuel starvation as a method of raising the anode potential. A PEMFC model for a different type of periodic pulsing, namely periodic pulsations in methanol feed concentration, was developed by Sundmacher et al. [18].

The first mathematical model of a PEMFC is often attributed to Bernardi and Verbrugge [19]. Since that time, several hundred models describing various aspects of PEMFCs have been formulated. Recently there have been several comprehensive reviews [20–23] of the various models.

A number of mathematical models have been developed to describe CO poisoning of PEM fuel cells. A steady state three-dimensional model was developed by Springer et al. [9] that successfully predicted the observed effects of CO on steady state polarization curves. Zhou and Liu [24] have also developed a three-dimensional model to describe PEMFC performance when operating with reformate that accounted for CO poisoning. A more comprehensive model has been developed by Baschuk and Li [25]. Both the model of Springer et al. [9] and that of Baschuk and Li [25] assume steady-state kinetics and are not suitable for simulating the transient phenomenon, such as spontaneous oscillations, that are associated with CO poisoning. Three-dimensional fluid dynamic models, such as that of Baschuk and Li [25], have however proved to be extremely useful for the optimization of design of fuel cells operating on pure hydrogen where the performance is often limited by mass transport within the cell. When the fuel contains significant levels of CO, the performance of the cell is generally limited by electrode kinetics.

Simplified zero-dimensional kinetic models have normally been used to simulate the transient effects of CO poisoning. In these models, the components in the anode chamber are typically assumed to be perfectly mixed so that the spatial non-uniformities within the cell that are associated with gas distribution and utilization are ignored. In this approach, a set of equations is written that describes the time dependence of the surface coverage of the adsorbed species, the mass balance in the anode chamber and the charge balance at the anode.

Bhatia and Wang [26] developed a simplified version of such a model to describe the slow poisoning and recovery of PEM fuel cells when exposed to carbon monoxide. Their model ignores the formation of adsorbed OH and the CO oxidation processes and is thus not capable of predicting the spontaneous oscillations in the fuel cell which result from self-cleaning when OH reacts with the adsorbed CO on the surface. Models similar to that of Bhatia and Wang have been developed by Zhang et al. [27] for CO poisoning and by Shi et al. [28] for poisoning by H_2S. Because of approximations such as neglect of CO oxidation, in their present form these models are not suitable for the simulation of some of the observed rapid transient behaviour such as spontaneous oscillations and the use of short current pulses to clean the anode.

A good understanding of the non-linear dynamics in electrochemical systems has been obtained through the recent work of Koper [29], Krischer [30] and Eisworth et al. [31]. Detailed analyses of potential oscillations during the electrooxidation of both CO [32] and formic acid [33,34] have been presented. More recently, Zhang et al. [4–6] have developed a dynamic model (hereafter referred to as "Zhang's model") for the anode of a PEM fuel cell operation on a hydrogen/CO mixture (reformate) based on the earlier work of Koper, Krisher and Eisworth et al. These authors have used this model to simulate the sustained potential oscillations observed in an operating PEM fuel cell. The kinetic parameters used in Zhang's model were derived from literature [9,32,35] as well as through fitting of experimental data.

One of the main goals of this study was to extend Zhang's model with the aim of using it to optimize the performance of a PEM fuel cell operating on reformate through the use of periodic pulsing. To provide data for model verification, we have measured the anode performance under a variety of conditions including anode polarization curves, galvanostatic measurement of sustained and transient oscillations and current pulsing. Initial tests of Zhang's model using his set of kinetic parameters showed that it did not simulate our results well. In an attempt to improve this model we have included the effects of mass transfer of reactants at the electrode and have adjusted some of the kinetic parameters.

2. Experimental

2.1. Cell and membrane electrode assembly

Experiments were made using a single electrochemical cell having a 25 cm^2 active area manufactured by ElectroChem Inc. The membrane electrode assembly (MEA) used in these experiments had a carbon supported platinum/ruthenium catalyst at both anode and cathode (loading: 1 mg Pt, 0.5 mg Ru cm^{-2}) and used Nafion^{TM} 115 as membrane material. All of the measurements were made at room temperatures (293 K). The cathode, operating in the hydrogen evolution mode [10], was used as a reference. Distilled water was circulated through the cathode compartment at 2.3 mL s^{-1} to ensure membrane humidification and to allow the cell temperature to be controlled. In this configuration, hydrogen gas was consumed at the anode and evolved at the cathode. A 1 atm operating pressure was maintained in the anode and cathode compartments.

2.2. Electrochemical measurements

A Kikusui Model PBX 20—10 Bi-Polar Power Supply, connected in parallel with the electrochemical cell, was used to control the cell current. The power supply was programmable so that the cell could be cycled through a predetermined current profile. A Fluke Hydra data logger was used to monitor and capture cell potential and current for final analyses using a desktop computer. One channel of the data logger was directly connected to the electrochemical cell to measure the cell potential while a second channel monitored cell current from a connection on the bipolar power supply. All of the polarization curve experiments were performed by ramping the current from 0 to 10 A at a rate of 20 mA s^{-1}. In the periodic pulsing experiments, the cell was run at a constant (base) current and, periodically, a variable width 10 A pulse was applied. By using the alarm function on the Fluke data logger, the pulse could be applied when the anode potential reached a predetermined value (designated as the "pulse initiation potential"). The transient potential data in the millisecond range were collected using a Nicolet 310 storage oscilloscope.

Pure hydrogen gas and a gas mixture of hydrogen and 1000-ppm CO were stored in high-pressure cylinders connected via small diameter plastic tubing to the fuel cell test station. The flow of the gases was controlled using calibrated rotameters mounted on the fuel cell test station. A constant input pressure of 140 kPa, upstream of the rotameter, was used. The total pressure in the anode and cathode compartments of the fuel cell was maintained at 1 atm. The total gas flow rate into the anode compartment of the electrochemical cell could be varied.

3. Results and discussion

3.1. Pure hydrogen

The uncorrected polarization curve for pure hydrogen gas flowing through the anode compartment and hydrogen purged distilled water flowing through the cathode compartment using a 25 cm^2 MEA catalyzed with platinum/ruthenium (1 mg Pt, 0.5 mg Ru cm^{-2}) is shown in Fig. 1. IR losses dominate the cell overpotential in the low current region of the curve. By taking the slope of the polarization curve in the 0.02–0.04 A cm^{-2} region, an estimate of 16.0 mΩ was obtained for the cell resistance. This resistance is about a factor of two higher than the value one obtains using the conductivity value that Dupont gives [36] in their technical literature for the conductivity and thickness

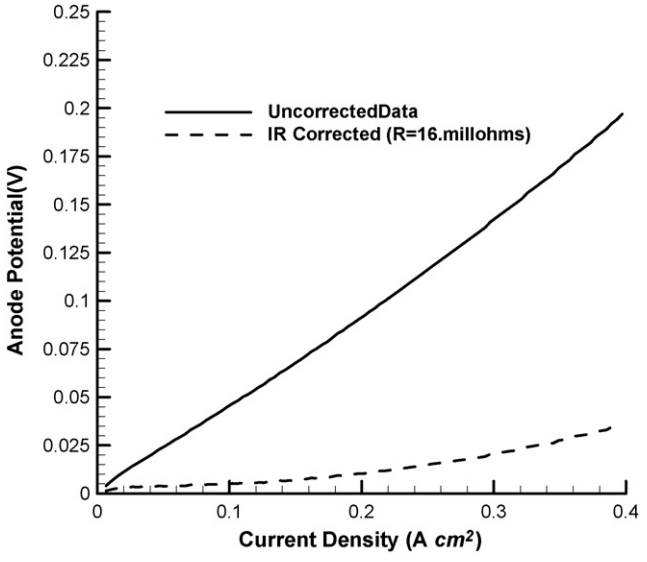

Fig. 1. Polarization curve for pure hydrogen gas at the anode (293 K, Pt/Ru catalyst, 3.25 mL s^{-1} gas flow, 1 atm).

of Nafion^{TM} 115. The extra resistance probably arises from the resistance of the thick graphite collector plates that are used in the cell as well as from contact resistance between the plates and the MEA.

The IR corrected polarization curve for the cell is also included in Fig. 1. The polarization curve has a distinct upward curvature indicating that, at the higher currents, mass transport contributes significantly to the overpotential. The curvature results from the difference in hydrogen partial pressures at the anode catalyst layer and the cathode catalyst layer. While the hydrogen pressure at the cathode remains constant at 1 atm, the hydrogen pressure at the anode drops because of the mass transfer resistance between the anode compartment (1 atm) and the anode catalyst layer (less than 1 atm). In Zhang's model, it is assumed that there is no mass transfer (diffusion) resistance and that the hydrogen pressure at the catalyst surface is the same as the bulk pressure in the anode chamber.

The corrected polarization curve shows that the maximum overpotential at the highest current density used in these experiments (0.4 A cm^{-2}) is about 20 mV. If it is assumed that this overpotential is divided equally between the anode and cathode, then the maximum overpotential at the cathode is 10 mV or less. The use of the cathode as a dynamic hydrogen reference electrode is thus justified since the overpotentials for the hydrogen/CO mixtures are much larger.

3.2. Hydrogen with 1000 ppm carbon monoxide

3.2.1. Polarization curve

Fig. 2 shows the uncorrected anode polarization curves for a 1000 ppm CO/hydrogen mixture with an input gas flow rate of 80 mL min^{-1}. The measurement was made at room temperature (293 K) with a total pressure at the anode and cathode of 1 atm. From this figure, we see that, because of the blockage of the active sites on the catalyst surface by CO, the anode potential rises quickly until it reaches a potential that is sufficiently high for the formation of adsorbed OH and so that oxidation of the adsorbed CO can occur (~500 mV). There is then a region (from ~0.05 to 0.15 A cm^{-2}) where the anode stays at the CO oxidation potential. Above a current density of about 0.15 A cm^{-2}, spontaneous oscillations of the anode potential start to occur.

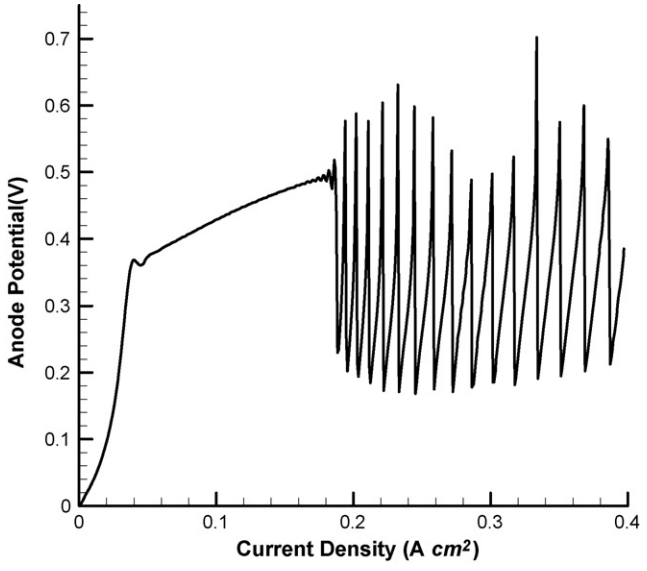

Fig. 2. Polarization curve for a 1000 ppm CO/H_2 gas mixture at the anode (293 K, Pt/Ru catalyst, 1.33 mL s^{-1} gas flow, 1 atm).

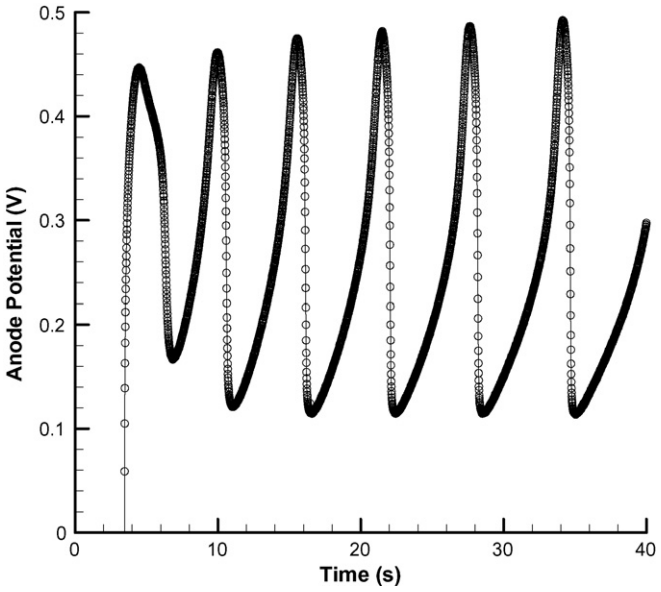

Fig. 3. Spontaneous oscillations in anode potential caused by a current step from 0 to 9 A (1000 ppm CO/H_2, 293 K, Pt/Ru catalyst, 2.0 mL s^{-1} gas flow, 1 atm).

3.2.2. Spontaneous oscillations

A detailed examination of the spontaneous oscillations in anode potential is given in Fig. 3. In this experiment, the cell remained at open circuit for a period of 10 min to allow the surface concentrations of CO and hydrogen to reach equilibrium values. The current was then stepped to 9 A. At this current, the anode potential rises rapidly and spontaneous oscillations occur. Under these conditions, the period of oscillation is about 5 s. From Fig. 3 it is seen that once the surface is cleaned through the reaction of the adsorbed CO with adsorbed OH, which forms at the higher anode potentials, the anode potential falls rapidly.

3.2.3. Transient oscillations

Fig. 4 illustrates the same process when a current of 4 A is used. Under these conditions transient rather than sustained oscillation are observed. These results are consistent with the polarization data given in Fig. 2 which shows that oscillations did not occur until the current was over 4 A under these conditions. It thus appears that the surface is initially blocked with CO and oscillations occur but, as the 4 A current flows, the surface concentration of CO moves toward the equilibrium value and the oscillations stop.

3.2.4. Anode regeneration by current pulsing

Even in the presence of 1000 ppm CO, the anode potential can be maintained at a relatively low value and the fuel cell efficiency can be significantly enhanced by periodically applying a short, high current pulse to raise the anode potential to clean the cata-

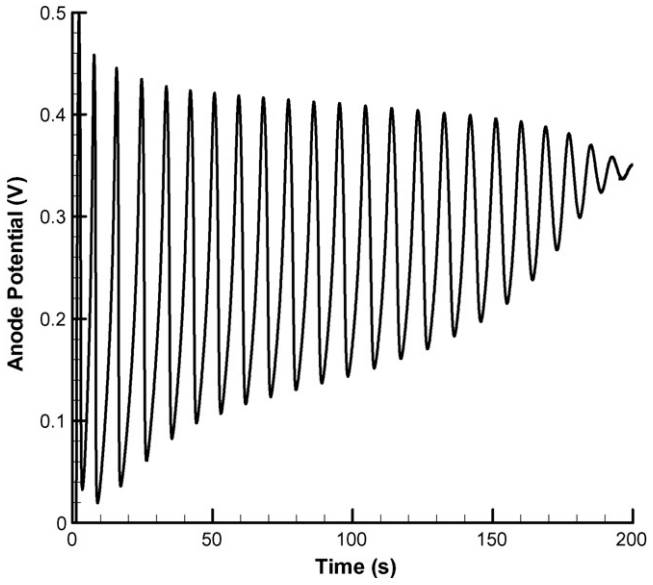

Fig. 4. Transient oscillations in anode potential caused by a current step from 0 to 4 A (1000 ppm CO/H_2, 293 K, Pt/Ru catalyst, 1.33 mL s^{-1} gas flow, 1 atm).

lyst surface. A detailed look at this process is shown in Fig. 5a and b for pulse initiation potentials of 0.3 and 0.4 V, respectively. In these experiments, a variable width, 10 A pulse was applied when the anode potential reached the preset value. A number of interesting features can be seen from these figures. When the current pulse is applied, the anode potential rises quickly until cleaning occurs and the anode potential falls rapidly. At a pulse initiation potential of 0.3 V, this process takes about 0.3 s whereas at 0.4 V it only takes about 0.2 s. Once the cleaning has taken place, from the data shown, it appears that extending the high current pulse is of little benefit and the energy used to extend the pulse after the surface is cleaned would be wasted. The data shows for the example, that the anode potential is essentially the same at 3 s regardless of whether 0.5 or 1 s pulse is applied. Fig. 5b shows similar data for a pulse initiation potential of 0.4 V.

The pulse initiation potential has a significant effect on the pulse width (pulse energy) required to regenerate the anode. The surface is less fouled at a lower anode potential and hence requires more energy to drive the anode to a sufficiently high potential to initiate cleaning. As an example, Fig. 6 shows in detail the behaviour at pulse initiation potentials of 0.19 and 0.225 V. At 0.19 V, a pulse width of about 1.5 s is required for regeneration while only about 0.6 s is required at 0.225 V. The choice of pulse initiation potential will clearly impact the efficiency of the regeneration process as is discussed below.

3.2.5. *Optimization of the efficiency of the pulsing process*

To measure the efficiency of the regeneration process, a series of experiments were carried out using different pulse initiation potentials. In these experiments, the cell remained at open circuit for 10 min to allow equilibrium conditions to be achieved at the surface. The pulsing process was then initiated and a further 10 min waited so that steady state was achieved before the data was collected using the Nicolet 310 transient oscilloscope. Typical results are shown in Fig. 7. From the data, it was observed

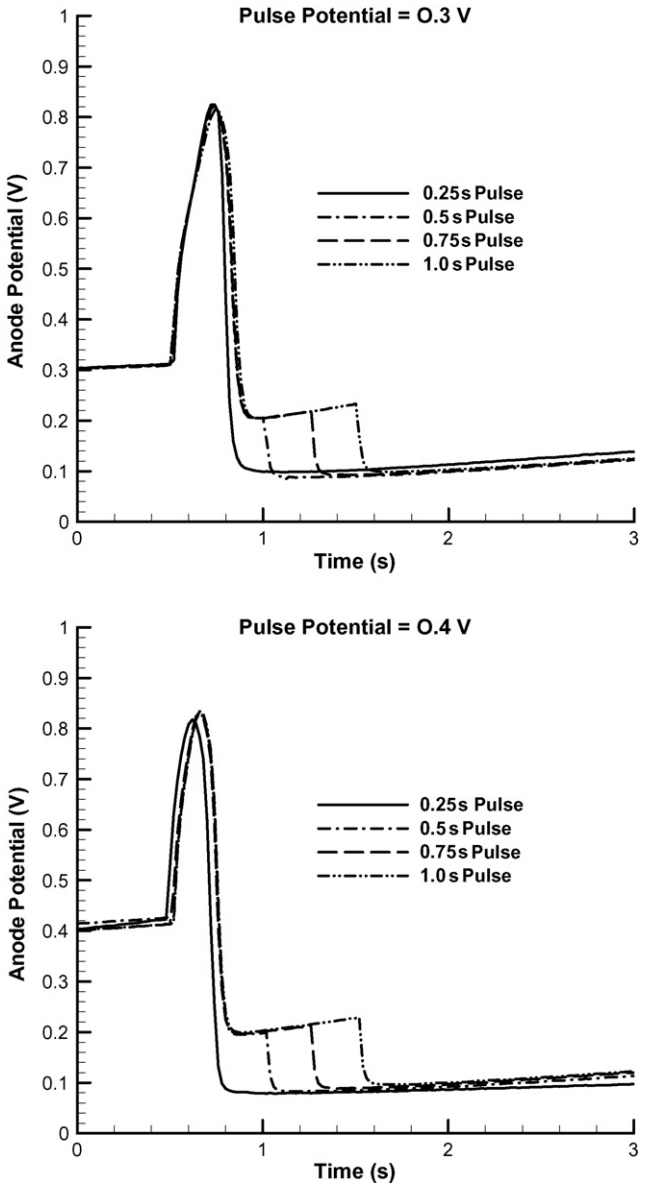

Fig. 5. The effect of pulse width on the anode potential of a CO-poisoned cell for two different pulse initiation potentials (1000 ppm CO/H_2, 293 K, Pt/Ru catalyst, 1.33 mL s^{-1} gas flow, 1 atm).

that the time required for anode regeneration as well as the time between pulses varied between adjacent pulses but was repeated in pairs. In this example, notice that the time between pulses 1 and 2 is shorter than that between pulses 2 and 3. In addition, a longer time is required for regeneration during pulse 1 than pulse 2. Note however that the regeneration times in pulses 1 and 3 are the same as are regeneration times in pulses 2 and 4. This behaviour was typical for all pulse potentials and is thought to result from the relatively slow (1 s) data collection rate of the Fluke data logger which controlled the pulsing of the cell. To calculate the effect of pulse initiation potential on regeneration efficiency, adjacent pairs of pulses were used.

The effect of pulse initiation potential on anode efficiency is illustrated in Fig. 8. Cell pulsing improves the anode efficiency by lowering the average working potential of the anode. The

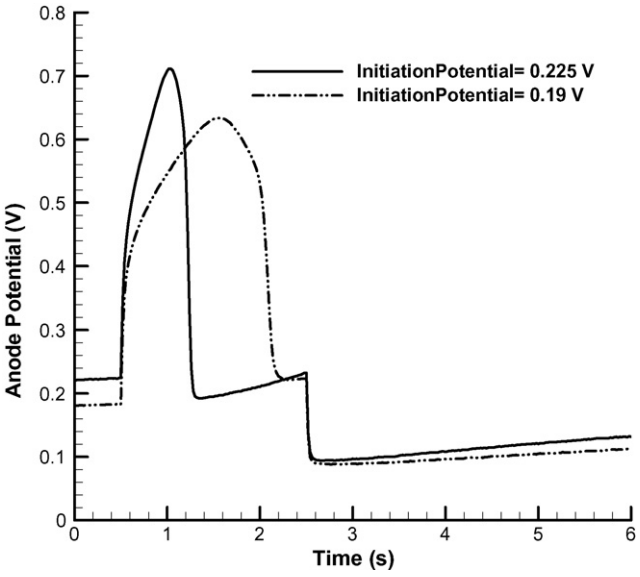

Fig. 6. The effect of pulse initiation potential on the anode potential of a CO-poisoned cell (1000 ppm CO/H_2, 293 K, Pt/Ru catalyst, 1.5 mL s^{-1} gas flow, 1 atm).

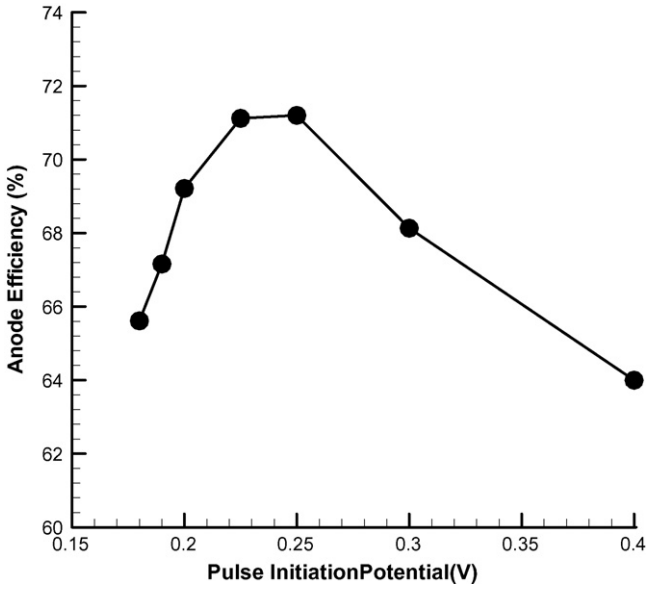

Fig. 8. The effect of pulse initiation potential on anode efficiency.

energy costs to achieve regeneration need to be consider in calculating the overall efficiency however. During pulsing, the cell is effectively shorted and during this period it provides no useful voltage. Fuel utilization is also higher during pulsing because of the higher current required. This source of inefficiency must also be included. Taking these effects into account and using experimental data collected at a number of pulse potentials, the anode efficiency curve shown in Fig. 8 is obtained. These efficiencies have been based on a "practical" anode potential of 0.75 which allows for significant cathode polarization. Use of a theoretical value of 1.23 V would have increased the calculated values. The data shows that, under our experimental conditions, optimal efficiency occurs when the cell is regenerated when the anode potential rises to about 0.25 V. At this pulse potential, the anode efficiency is about 71%. This can be compared to an anode efficiency of only 36% if the cell is operated without pulsing using hydrogen containing 1000 ppm CO. Under these operating conditions the anode potential rises to about 0.48 V.

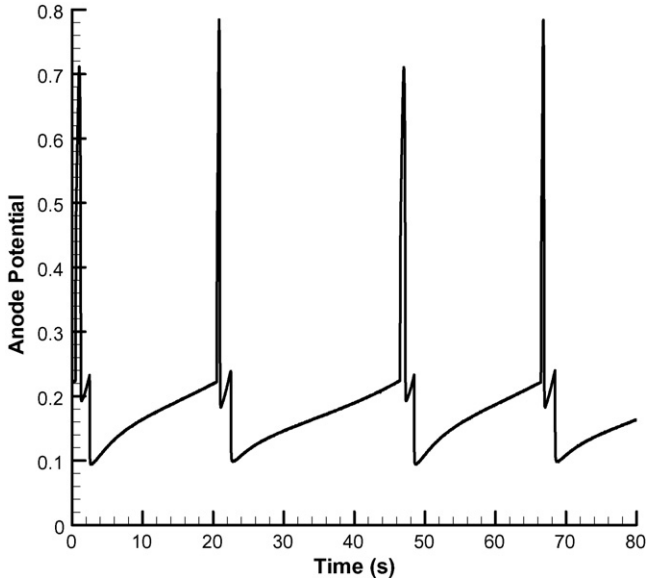

Fig. 7. The effect of pulsing on the anode potential of a CO-poisoned cell showing several current pulses (1000 ppm CO/H_2, 293 K, Pt/Ru catalyst, 1.5 mL s^{-1} gas flow, 1 atm).

4. Modelling CO poisoning of the anode

4.1. Development of the model

To model CO poisoning of the anode, a modified version of the procedure used by Zhang et al. [4,6] was used. As discussed in Section 3.1, the hydrogen polarization data indicates that there is considerable resistance to the mass transfer of hydrogen and CO to the surface of the electrode which is unaccounted for in Zhang's model. The exact source of this resistance to the diffusion of hydrogen and CO to the surface is uncertain but it could result from the gas diffusion layer, the catalyst layer or in a water layer surrounding the catalyst.

To avoid repeating much of the material already published, the reader is referred to the work of Zhang et al. [4,6]. In the development of our model, Eqs. (1)–(3) and (5) of Zhang's model are maintained, however any term expressed in concentration is converted to partial pressure using the ideal gas law and gas pressures at the surface, rather than gas pressures in the bulk, were used. Zhang's equation (4) is eliminated because it intrinsically assumes that the hydrogen and CO pressures in the bulk and at the surface are identical (i.e. there is no diffusion resistance). Zhang's equation (4) is therefore replaced by three new equations expressing the rate of change of: (a) CO pressure at the surface; (b) CO pressure in the bulk; (c) hydrogen pressure at the surface. The partial pressure of the hydrogen in the bulk of the anode chamber is assumed constant and equal to the total pressure in the anode chamber

(1 atm) since the partial pressure of CO is negligible. The anode chamber is assumed to be well stirred which allows a one-dimensional model to be used. Zhang's use of mass balance and his expressions for the reaction rates are retained in this model.

To create an expression for the rate of change of the partial pressure of species i at the surface of the catalyst with respect to time the mass balance at the catalyst surface must be calculated. This yields

$$\frac{dC_i^s}{dt} = N_i A - \frac{r_{i,ads} A}{n_i F} \quad (6)$$

All of the symbols used in this section are defined in Table 1. The first term of this equation represents the flux of species i from the anode chamber to the surface by diffusion and the second term represents the removal of species i by adsorption onto the catalyst surface. In our model, the following simple Fick's law equation for mass transfer that assumes a linear concentration gradient across the diffusion layer has been used:

$$N_i = \frac{D_i(C_i^b - C_i^s)}{h} \quad (7)$$

Thus, Eq. (6) becomes

$$\frac{dC_i^s}{dt} = \frac{D_i A(C_i^b - C_i^s)}{h} - \frac{r_{i,ads} A}{n_i F} \quad (8)$$

Conversion of the concentration terms to partial pressures using the ideal gas and Dalton's law then gives

$$\frac{dp_i^s}{dt} = \frac{D_i A(p_i^b - p_i^s)}{h} - \frac{r_{i,ads} ART}{n_i F} \quad (9)$$

Specific expressions for the rate of change of the hydrogen and carbon monoxide pressures at the surface then become

$$\frac{dp_H^s}{dt} = \frac{D_H A(p_H^b - p_H^s)}{h} - \frac{r_{H,ads} ART}{2F} \quad (10)$$

and

$$\frac{dp_{CO}^s}{dt} = \frac{D_{CO} A(p_{CO}^b - p_{CO}^s)}{h} - \frac{r_{CO,ads} ART}{F} \quad (11)$$

These are two of the additional ordinary differential equations that need to be solved and that replace Zhang's equation (4). A final equation is needed for the rate of change of the partial pressure of CO in the anode chamber. To obtain this equation a similar mass balance approach is taken. The rate of change of species i in the anode chamber can be written as

$$V_A \frac{dC_i^b}{dt} = \nu_0 C_i^0 - \nu C_i^b - N_i A \quad (12)$$

The first two terms on the right-hand side of this equation represent the flow of species i into and out of the anode chamber respectively and the last term represents diffusion of species i to the surface. Converting from concentration to pressure as before and noting that $dp_H/dt = 0$ then leads to the following equation

Table 1
Symbol definitions and parameter values

Symbol	Meaning	Value	Units
K_{CO}	CO equilibrium rate constant for desorption	8.8×10^{-6}	atm
K_H	H equilibrium rate constant for desorption	0.5	atm
$\vec{k}_{CO,ads}$	Forward rate constant for CO adsorption	192.	A cm^{-2} atm
$\vec{k}_{CO,ox}$	Forward rate constant for CO oxidation	5.5×10^{-4}	A cm^{-2}
$\vec{k}_{H,ads}$	Forward rate constant for H adsorption	4000	A cm^{-2} atm
$\vec{k}_{H,ox}$	Forward rate constant for H oxidation	4	A cm^{-2}
$\overleftarrow{k}_{OH}$	Backward rate constant for OH formation	2760	A cm^{-2}
$\vec{k}_{OH}$	Forward rate constant for OH formation	8×10^{-4}	A cm^{-2}
θ_0	Fraction of free catalyst surface sites	Variable	
θ_{CO}	CO surface coverage	Variable	
θ_H	H surface coverage	Variable	
θ_{OH}	OH surface coverage	Variable	
p_H^b	Bulk hydrogen pressure	1	atm
p_H^s	Hydrogen pressure at the surface	Variable	atm
p_{CO}^b	Bulk carbon monoxide pressure	Variable	atm
p_{CO}^s	Carbon monoxide pressure at the surface	Variable	atm
C_H^b	Hydrogen concentration in anode chamber	0.12	mol L^{-1}
C_H^s	Hydrogen concentration at the surface	Variable	mol L^{-1}
C_{CO}^b	Carbon monoxide concentration in anode chamber	Variable	mol L^{-1}
C_{CO}^s	Carbon monoxide concentration at the surface	Variable	mol L^{-1}
η_A	Anode overpotential	Variable	V
N_{CO}	CO gas flux		
N_H	Hydrogen gas flux		
$r_{CO,ox}$	Rate of CO oxidation	Variable	mol s^{-1}
$r_{CO,ads}$	Rate of CO adsorption	Variable	mol s^{-1}
$r_{H,ox}$	Rate of H oxidation	Variable	mol s^{-1}
$r_{H,ads}$	Rate of H adsorption	Variable	mol s^{-1}
r_{OH}	Net rate of water dissociation	Variable	mol s^{-1}
A	Total catalyst surface area	25	cm^2
C_t	Atom mole density per catalyst surface area	2.2×10^{-9}	mol cm^{-2}
C_{dl}	Anode double layer capacity	0.45	F
γ	Anode roughness factor	100	
V_A	Anode chamber volume	4.4	cm^3
ν_0	Inlet gas flow rate	Variable	mL s^{-1}
ν	Exit gas flow rate	Variable	mL s^{-1}
I	Current density	Variable	A cm^{-2}
D_{CO}	CO gas diffusivity	Variable	cm^2 s^{-1}
D_H	H_2 gas diffusivity	Variable	cm^2 s^{-1}
h	Thickness of the gas diffusion layer	Variable	cm
T	Temperature	293	K
F	Faraday's constant	96,500	C mol^{-1}
R	Gas constant	8.314	L atm mol^{-1}
α	Transfer coefficient	0.5	
a	Constant = $\alpha F/RT$	19.48	V^{-1}
Q	Constant = $F\gamma C_t$	0.021	C cm^{-2}
n_i	Number of electrons		

for the rate of change of CO pressure in the anode chamber

$$\frac{dp_{CO}^{b}}{dt} = \frac{\nu_0 p_{CO}^{0}}{V_A} - \frac{\nu_0 p_{CO}^{b}}{V_A} + \frac{D_H A(p_H^0 - p_H^s)p_{CO}^{b}}{V_A p_H^0} - \frac{D_{CO}A(p_{CO}^0 - p_{CO}^s)}{V_A} \quad (13)$$

This is the final equation that is required for the model. It should be noted that transport of the carbon dioxide product away from the surface is ignored in this model.

Once the constants in the equations are grouped equation, the seven equations used for the model can be written as

$$\frac{d\theta_{CO}}{dt} = A_3[p_{CO}^s(1-\theta_{CO}-\theta_H-\theta_{OH}) - K_{CO}\theta_{CO}] - A_4\theta_{CO}\theta_{OH}\exp(\alpha\eta_A) \quad (14)$$

$$\frac{d\theta_H}{dt} = A_2[p_H^s(1-\theta_{CO}-\theta_H-\theta_{OH})^2 - K_H\theta_H^2] - 2A_1\theta_H \sin h(\alpha\eta_A) \quad (15)$$

$$\frac{d\theta_{OH}}{dt} = A_5(1-\theta_{CO}-\theta_H-\theta_{OH})\exp(\alpha\eta_A) - A_6\theta_{OH}\exp(-\alpha\eta_A) - A_4\theta_{CO}\theta_{OH}\exp(\alpha\eta_A) \quad (16)$$

$$\frac{dp_{CO}^{b}}{dt} = \frac{Nu}{V}(XP - p_{CO}^{b}) + \frac{A_7 A p_{CO}^{b}}{V}\left(1 - \frac{p_H^s}{P}\right) - \frac{A_8 A}{V}(p_{CO}^{b} - p_{CO}^{s}) \quad (17)$$

$$\frac{dp_H^s}{dt} = A_7 A(P - p_H^s) - \frac{RTAk_{H,ad}}{2F}[p_H^s(1-\theta_{CO}-\theta_H-\theta_{OH})^2 - K_H\theta_H^2] \quad (18)$$

$$\frac{dp_{CO}^{s}}{dt} = A_8 A(p_{CO}^{b} - p_{CO}^{s}) - \frac{RTA\vec{k}_{CO,ad}}{F}[p_{CO}^{s}(1-\theta_{CO} - \theta_H - \theta_{OH}) - K_{CO}\theta_{CO}] \quad (19)$$

$$\frac{d\eta_A}{dt} = A_9[I(t) - 2k_{H,ox}\theta_H \sin h(\alpha\eta_A) - \vec{k}_{CO,ox}\theta_{CO}\theta_{OH}\exp(\alpha\eta_A) - \vec{k}_{OH}(1-\theta_{CO}-\theta_H-\theta_{OH}) \times \exp(\alpha\eta_A) + \vec{k}_{OH}\theta_{OH}\exp(-\alpha\eta_A)] \quad (20)$$

Table 2
Model parameters

Symbol	Meaning	Value	Units
A_1	Constant $= \vec{k}_{H,ox}/Q$	190.48	s^{-1}
A_2	Constant $= \vec{k}_{H,ads}/Q$	1.9×10^5	$(atm\,s)^{-1}$
A_3	Constant $= \vec{k}_{CO,ads}/Q$	9143	$(atm\,s)^{-1}$
A_4	Constant $= \vec{k}_{CO,ox}/Q$	0.0262	s^{-1}
A_5	Constant $= \vec{k}_{OH}/Q$	0.0381	s^{-1}
A_6	Constant $= \vec{k}_{OH}/Q$	1.3×10^5	s^{-1}
A_7	Constant $= D_H/h$	5.8×10^{-2}	$cm\,s^{-1}$
A_8	Constant $= D_{CO}/h$	1.6×10^{-2}	$cm\,s^{-1}$
A_9	Constant $= A/C_{dl}$	55.56	$cm^2\,F^{-1}$

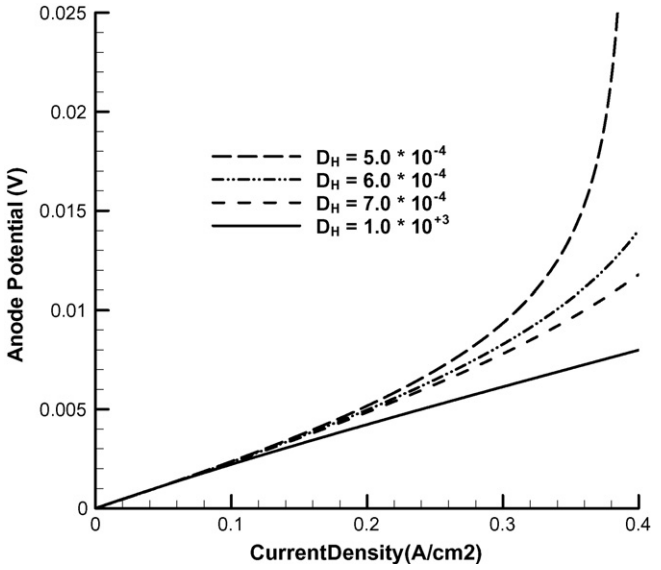

Fig. 9. Calculated polarization curves for pure hydrogen for various values of hydrogen diffusion coefficient (293 K, 2.0 mL s^{-1} gas flow, 1 atm).

Table 2 identifies and gives values for all of the parameters used in this model. As will be discussed later, we found it necessary to adjust some of the kinetic parameters given by Zhang et al. [4,6] to obtain a reasonable fit to our data. This set of seven ordinary differential equations (ODEs) was solved using the ODE solver in Scilab©[37]. Separate programs were written to simulate the constant current, current sweep and current pulse experiments.

To validate the seven-equation model, the results from this model were compared to the results from Zhang's model at two limiting conditions where the models were expected to give the same results. Firstly, equilibrium surface coverages and gas pressures were calculated under open circuit conditions where the net reaction rate is zero and therefore the rate of diffusion will

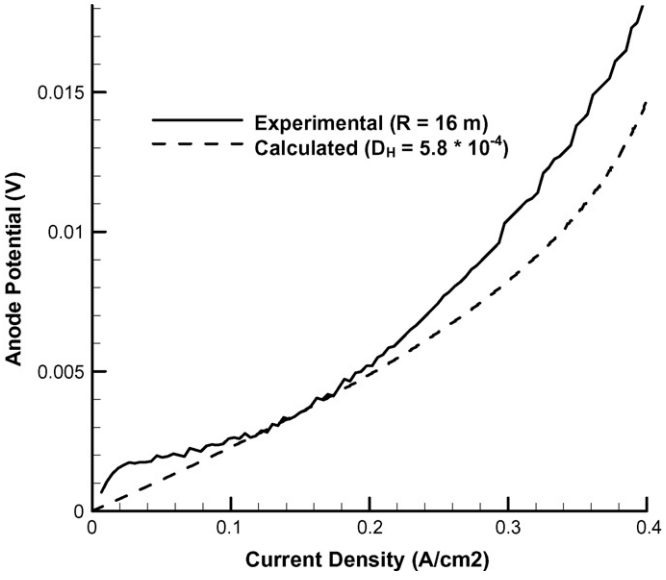

Fig. 10. Comparison of experimental and calculated anode polarization curves for pure hydrogen.

also be zero and, secondly, the response to a step in current was calculated assuming a large value for the diffusion constant so there was no mass transfer limitation. In both cases, the results from the two models were found to be essentially identical.

4.2. Determination of the diffusion constants from the hydrogen polarization curve

To estimate the diffusion coefficient, a series of polarization curves were calculated using the seven-equation model using $p^{b}_{CO} = 0$ and various values for D_H/h. As mentioned earlier, the source of the diffusion resistance is unclear but could arise in the gas diffusion layer, solid-state diffusion in the catalyst layer or, possibly, diffusion through a water film surrounding the catalyst. The results (Fig. 9) show that, for a large value of D_H, the slightly convex polarization curve has Butler–Volmer type behaviour. As the diffusion coefficient is made smaller however, the increasing diffusion resistance introduces upward curvature into the polarization curves as a result of the limited rate of mass transport of hydrogen to the surface. Based on a comparison (Fig. 10) of the experimental data with the calculated polarization curves, a rough estimate of $D_H/h = 5.8 \times 10^{-2}$ was obtained. To obtain the experimental polarization curve for the anode, it was assumed that the polarization was equally split between anode and cathode. A cell resistance value of 16 mΩ was used.

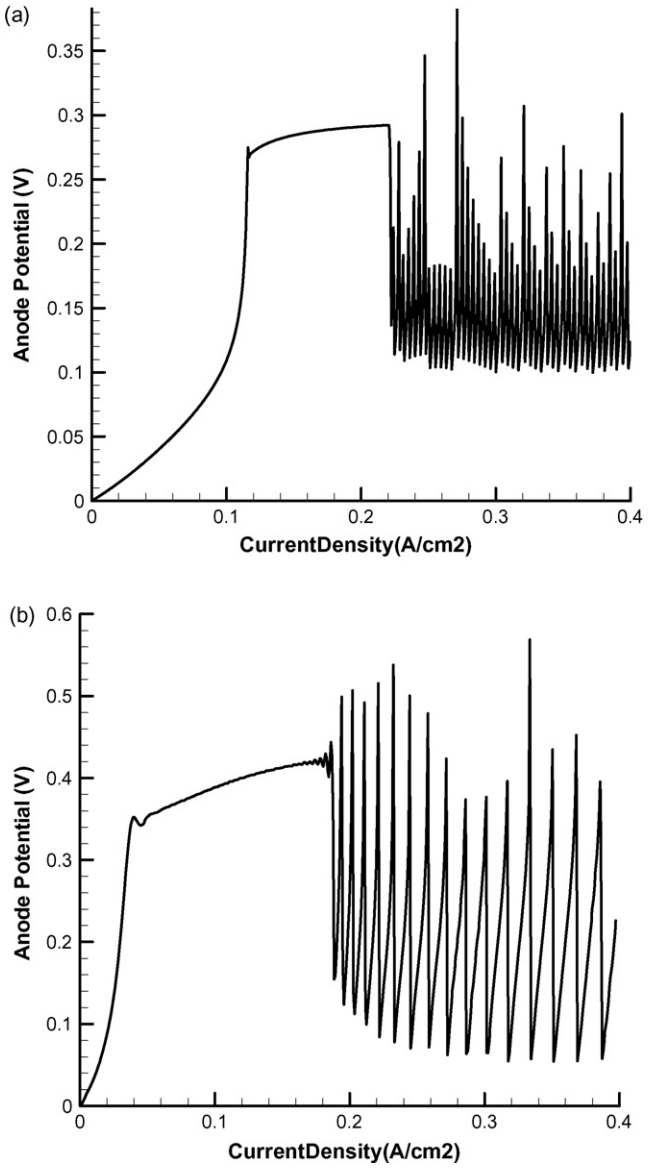

Fig. 11. Comparison of calculated and experimental polarization curves for a 1000 ppm CO/H_2 gas mixture (1000 ppm CO/H_2, 1.33 mL s^{-1} gas flow, 1 atm).

4.3. Polarization curve for a 1000 ppm CO/hydrogen mixture

The polarization curve for a 1000 ppm CO/hydrogen mixture was calculated using the parameters given in Table 2. Initial tests using the kinetic parameters given by Zhang et al. [6] gave poor results. With Zhang's model, spontaneous oscillations were observed as soon as current flow was initiated—a result that is not in agreement with experiment (Fig. 2). It was concluded that Zhang's parameters resulted in the surface being almost completely blocked by CO leaving very little surface available for the electrooxidation of hydrogen. To overcome this difficulty, we have increased the value of both K_{CO} and $k_{H,ads}$ by about an order of magnitude in our model. A minor change was also made to $k_{CO,ads}$. Using these parameters, it is seen that there is good qualitative agreement between the shape of the calculated polarization curve (Fig. 11a) and the shape of the IR corrected experimental polarization curve (Fig. 11b).

4.4. Simulation of spontaneous and transient oscillations

Experimentally, spontaneous oscillations occur under a variety of conditions in the CO/hydrogen system. From the polarization curve of Fig. 2, oscillations are expected at high

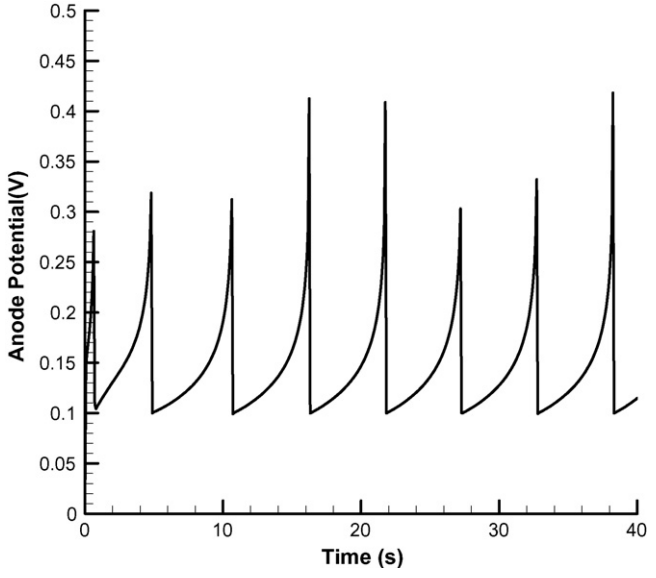

Fig. 12. Calculated results for the spontaneous oscillations in anode potential caused by a current step from 0 to 9 A (1000 ppm CO/H_2, 2.0 mL s^{-1} gas flow, 1 atm).

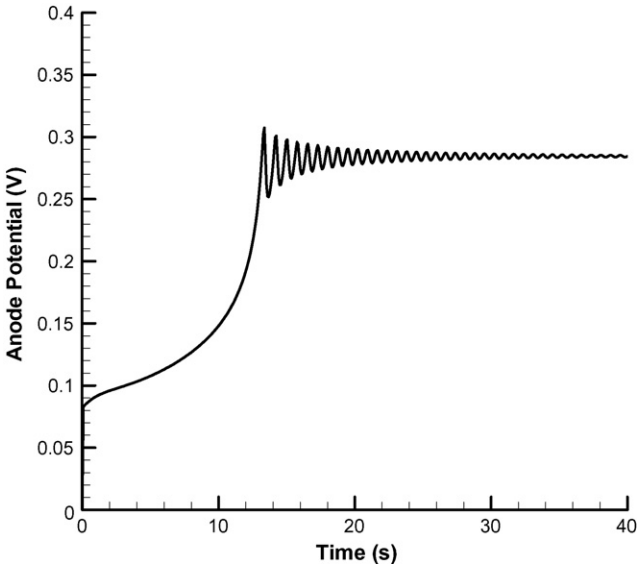

Fig. 13. Calculated results for the transient oscillations in anode potential caused by a current step from 0 to 4 A (1000 ppm CO/H_2, 1.33 mL s^{-1} gas flow, 1 atm).

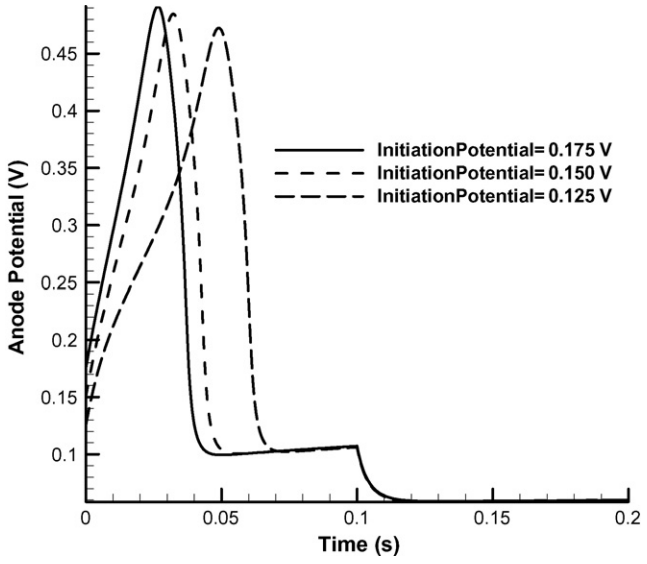

Fig. 14. Calculated results for the effect of pulse initiation potential on anode response to a 10 A pulse (1000 ppm CO/H_2, 1.33 mL s^{-1} gas flow, 1 atm).

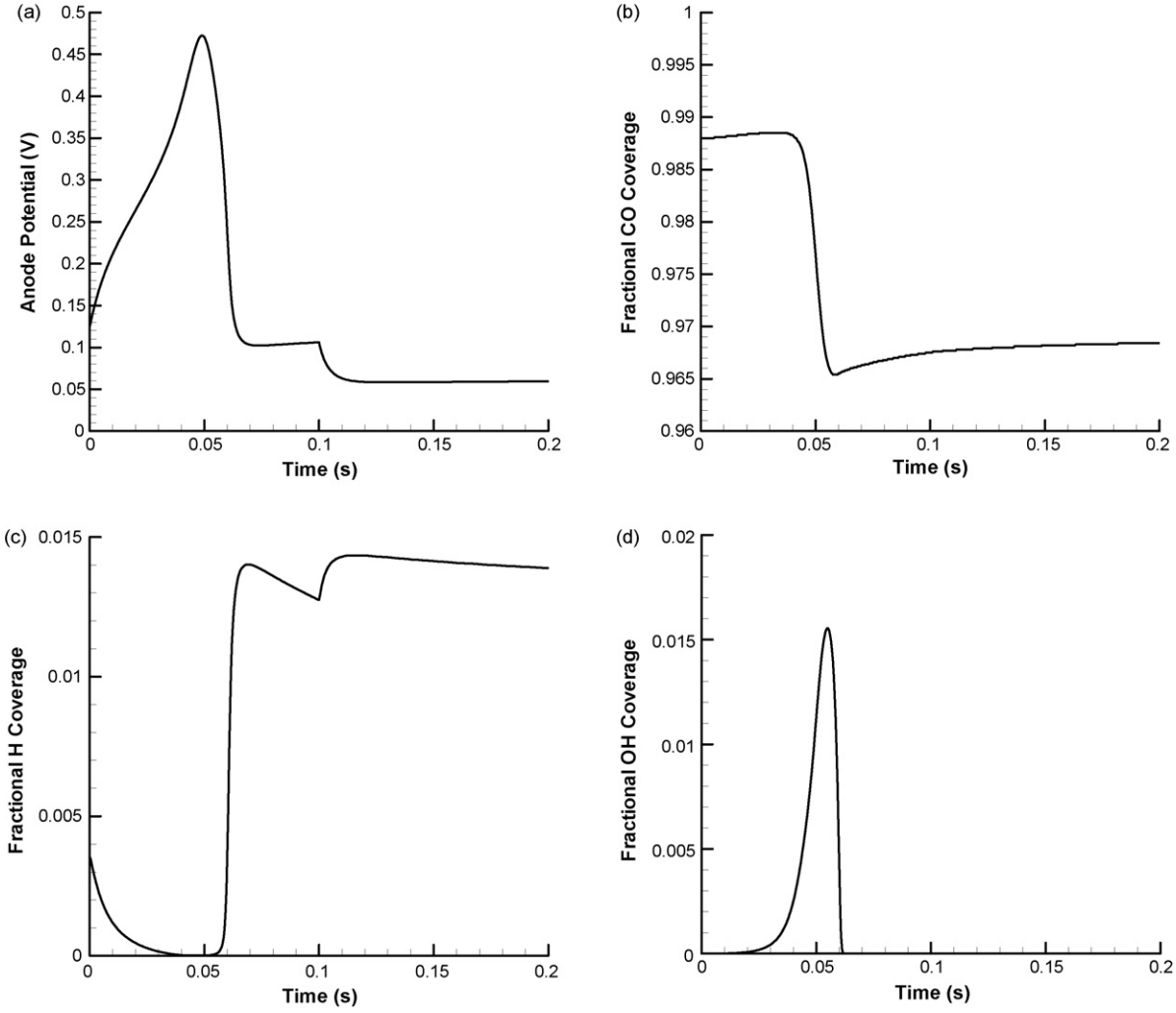

Fig. 15. Results showing the effect of applying a 10 A current pulse on: (a) the anode potential and (b) the surface coverage of CO, (c) the surface coverage of H and (d) the surface coverage of OH (1000 ppm CO/H_2, 1.33 mL s^{-1} gas flow, 1 atm).

currents. Fig. 3 shows the oscillations that are obtained when the current is stepped from 0 to 9 A. Simulation of these oscillations was attempted using the seven-equation model and the results are shown in Fig. 12. In general, the simulation is in good agreement with the experimental results. Comparison of Fig. 12 with Fig. 3 shows that the period and amplitude of the oscillations are very similar. At lower currents (e.g. 4 A) the oscillations are found to be evanescent (Fig. 4). The calculated response to a 4 A current step, shown in Fig. 13, also shows that damped oscillations occur although the onset and amplitude of the oscillations are not in exact agreement. The model is successful in that it predicts both that oscillations will begin and that they will eventually be damped to extinction.

4.5. Simulation of anode regeneration by current pulsing

Experimental results showing the use of current pulsing for the removal of CO and anode regeneration were presented in Section 3.4. The use of current pulsing can reduce substantially the average anode potential and increase fuel cell efficiency. Calculated results for the effect of pulsing for several pulse initiation potentials are shown in Fig. 14. For this calculation, the base current was set at 4 A with a pulse current of 10 A. To vary the pulse initiation potential, initial conditions corresponding to various potentials were fed into the model using the data shown in Fig. 13 (i.e. a 4 A current was applied and the current pulse initiated when the anode potential had risen to the desired value). The calculated results are seen to be in qualitative agreement with the experiments. They show, for example, that the time needed for cleaning increases as the pulse initiation potential is reduced. In general, however, the calculated times needed for cleaning are shorter than those measured experimentally.

Examination of the modelling results provides a clear insight into the regeneration process. In Fig. 15, we have shown predictions by the model for the anode potential as well as for the surface coverages of CO, H and OH when a 10 A pulse is applied. The results show that as the anode potential (Fig. 15a) rises, a significant concentration of adsorbed OH is formed (Fig. 15d). Rapid reaction of this OH with the adsorbed CO reduces the coverage of CO on the surface (Fig. 15b) which allows hydrogen coverage to increase (Fig. 15c). When more electrode surface area is available for the electrooxidation of hydrogen, the anode potential falls. Note that, in agreement with the experimental results, cleaning occurs before the end of the pulse.

4.6. Discussion

To achieve agreement between the experimental results and the modelling results, we have found it necessary to adjust a number of the kinetic parameters used earlier by Zhang et al. [6]. The number of adjustable parameters required in this model is large. To have a high level of confidence in the parameters selected, the measurement of additional parameters (e.g. CO pressure and/or surface coverages) and over a wider range of experimental conditions (e.g. temperature, pressure and gas composition) is going to be needed.

5. Conclusions

It is well known that CO poisoning of PEM fuel cells caused by even trace amounts of CO in the hydrogen fuel can lead to significant performance degradation and, under certain conditions, can lead to electrochemical oscillations in a fuel cell. A number of techniques have been developed to help alleviate this poisoning problem. One of the more recent techniques that have been developed is the use of pulsing to periodically raise the anode potential to clean the catalyst surface and raise the average cell operating potential thereby increasing fuel cell efficiency.

In this paper, we present a range of experimental results related to the CO-poisoning and cleaning of the anode of a fuel cell using a platinum/ruthenium catalyst. These results include cell polarization curves, measurements of spontaneous and transient oscillations of the anode potential and a detailed examination of cell behaviour during current pulsing. The current pulsing results showed that once the anode potential has been raised high enough for CO stripping to occur and, subsequently, the anode potential has dropped, the passage of further high current serves no useful purpose and, in fact, will only reduce fuel cell efficiency. To optimize fuel cell efficiency, it has also been shown that the choice of cell potential for the initiation of cell pulsing is important. In general, there will be a pulse initiation potential that optimizes the trade-off between the benefit gained by reducing the normal operating anode potential and the parasitic energy required for the pulsing process.

The development of a mathematical model to understand and control the poisoning and cleaning processes is considered desirable and was one of the goals of this study. In this paper, we have extended the model of Zhang et al. [6] to include mass transfer effects, something that our polarization results with pure hydrogen showed to be important. We have shown that the new model gives results that are in reasonable agreement with experiment over a fairly broad range of experiments.

Acknowledgements

The authors gratefully acknowledge funding from the Canadian Government's Natural Sciences and Engineering Research Council.

References

[1] J.J. Baschuk, X. Li, Int. J. Energy Res. 25 (2001) 695.
[2] X. Cheng, Z. Shi, N. Glass, L. Zhang, J. Zhang, D. Song, Z.-S. Liu, H. Wang, J. Shen, J. Power Sources 165 (2007) 739.
[3] H.F. Oetjen, V.M. Schmidt, U. Stimming, F. Trila, J. Electrochem. Soc. 143 (1996) 3838.
[4] J. Zhang, Investigation of CO tolerance in proton exchange membrane fuel cells, PhD thesis, Worcester Polytechnic Institute, June, 2004.
[5] J. Zhang, R. Datta, J. Electrochem. Soc. 149 (2002) A1423.
[6] J. Zhang, J.D. Fehribach, R. Datta, J. Electrochem. Soc. 151 (2004) A689.
[7] H.A. Gasteiger, N.M. Markovic, P.N. Ross, J. Phys. Chem. 99 (1995) 8290.
[8] H.A. Gasteiger, N.M. Markovic, P.N. Ross, J. Phys. Chem. 99 (1995) 16757.
[9] T.E. Springer, T. Rockward, T.A. Zawodzinski, S. Gottesfeld, J. Electrochem. Soc. 148 (2001) A11.

[10] D.C. Papageorgopoulos, F.A. de Bruijn, J. Electrochem. Soc. 149 (2002) A140.
[11] S. Gottesfeld, J. Pafford, J. Electrochem. Soc. 135 (1988) 2651.
[12] S. Gottesfeld, US Patent 4,910,099 (1990).
[13] T. Iorio, K. Yasuda, Z. Siroma, N. Fujiwara, Y. Miyazaki, J. Electrochem. Soc. 150 (2003) A1225.
[14] L.P. Carrette, K.A. Friedrich, M. Huber, U. Stimming, Phys. Chem. Chem. Phys. 3 (2001) 320.
[15] S. Wasmus, A. Kuver, J. Electroanal. Chem. 461 (1999) 14.
[16] W.A. Adams, J. Blair, K.R. Bullock, C.L. Gardner, J. Power Sources 145 (2004) 55.
[17] D.P. Wilkinson, C. Chow, D. Allan, E. Johannes, J. Roberts, J. St. Pierre, C. Longley, J. Chan, US Patent 6,096,448 (2000).
[18] K. Sundmacher, T. Schulz, S. Zhou, K. Scott, M. Ginkel, E.D. Gilles, Chem. Eng. Sci. 56 (2001) 333.
[19] D.M. Bernardi, M.W. Verbrugge, AIChE J. 37 (1991) 1151.
[20] K.Z. Yao, K. Karan, K.B. McAuley, P. Oosthuizen, B. Peppley, T. Xie, Fuel Cells 4 (2004) 3.
[21] D.R. Sousa, E.R. Gonzalez, J. Power Sources 157 (2005) 32.
[22] D. Cheddie, N. Munroe, J. Power Sources 147 (2005) 72.
[23] A. Biyikoglu, Int. J. Hydrogen Energy 30 (2005) 1181.
[24] T. Zhou, H. Liu, J. Power Sources 138 (2004) 101.
[25] J.J. Baschuk, X. Li, J. Power Sources 142 (2004) 134.
[26] K.K. Bhatia, C.-Y. Wang, Electrochim. Acta 49 (2004) 2333.
[27] J. Zhang, H. Wang, D.P. Wilkinson, D. Song, J. Shen, Z.-S. Liu, J. Power Sources 147 (2005) 58.
[28] Z. Shi, D. Song, J. Zhang, Z.-S. Liu, S. Knights, R. Vohra, N.Y. Jia, D. Harvey, J. Electrochem. Soc. 154 (2007) B609.
[29] M. Koper, J. Chem. Soc., Faraday Trans. 94 (1998) 1369.
[30] K. Krischer, in: J.O'M. Bockris, B.E. Conway, R.E. White (Eds.), Modern Aspects of Electrochemistry, Plenum Press, New York, 1998.
[31] M. Eiswirth, J. Burger, P. Strasser, G. Ertl, J. Phys. Chem. 100 (1996) 19118.
[32] M. Koper, T.J. Schmidt, N.M. Markovic, P.N. Ross, J. Phys. Chem. B 105 (2001) 8381.
[33] P. Strasser, M. Lubke, F. Raspel, M. Eiswirth, G. Ertl, J. Chem. Phys. 107 (1997) 979.
[34] P. Strasser, M. Eiswirth, G. Ertl, J. Chem. Phys. 107 (1997) 991.
[35] M.C. Deibert, D.L. Williams, J. Electrochem. Soc. 116 (1969) 1291.
[36] www.dupont.com/fuelcells/pdf/dfc101.pdf.
[37] www.scilab.org.